Ion-Molecule Reactions of ArN_2^+ with Butane and Isobutane at Thermal Energy

Masaharu TSUJI,*,†,†† Ken-ichi MATSUMURA,†† Hiroyuki KOUNO,††
Tsuyoshi FUNATSU,†† and Yukio NISHIMURA†,††
† Institute of Advanced Material Study, Kyushu University, Kasuga, Fukuoka 816
†† Department of Molecular Science and Technology, Graduate School of Engineering Sciences, Kyushu University, Kasuga, Fukuoka 816

(Received February 7, 1994)

Product ion distributions and rate constants have been determined for thermal energy reactions of ArN_2^+ with n-C_4H_{10} and i-C_4H_{10} by using an ion-beam apparatus. $C_4H_9^+$, $C_3H_n^+$ (n=5—7), and $C_2H_n^+$ (n=4,5) are produced from n-C_4H_{10} with branching ratios of 6, 57, and 37%, while $C_4H_9^+$ and $C_3H_n^+$ (n=5—7) are formed from i-C_4H_{10} with branching ratios of 13 and 87%, respectively. A comparison of the product ion distribution in the ArN_2^+/n-C_4H_{10} reaction with that predicted from the fragmentation pattern of n-$C_4H_{10}^+$ suggests that most of all fragment ions are formed through (pre)dissociation of precursor n-$C_4H_{10}^+$ states at ca. 13.2 eV. Since this energy is close to the effective recombination energy of ArN_2^+ (ca. 13.5 eV), it is concluded that the ArN_2^+/n-C_4H_{10} dissociative charge-transfer reaction proceeds through near-resonant n-$C_4H_{10}^+$ states. The total rate constants are $(6.9\pm2.3)\times10^{-10}$ $cm^3\,s^{-1}$ for n-C_4H_{10} and $(9.0\pm2.6)\times10^{-10}$ $cm^3\,s^{-1}$ for i-C_4H_{10}, which amount to 58 and 75% of the collision rate constants estimated from Langevin theory, respectively.

The attention that simple cluster ions with a N_2 molecule has received in recent years is partly due to their important role in the chemistry of the upper atmosphere.[1] The simple Ar_2^+, ArN_2^+, and N_4^+ cluster ions have nearly the same recombination energies of 14.518±0.017, 14.51, and 14.50±0.08 eV, respectively,[2—5] because the recombination energies (RE's) of Ar^+ ($^2P_{3/2}$: 15.76 eV) and N_2^+ (15.58 eV) are similar, and the binding energies of these ionic clusters are similar. It is known that there is a significant difference in the reactivity between homo-molecular Ar_2^+ and $(N_2)_2^+$ cluster ions for CH_4. Only charge-transfer (CT) channel leading to the parent CH_4^+ ion is found in the Ar_2^+/CH_4 reaction,[6] while both CT and displacement reaction leading to $N_2CH_4^+$ are found in the N_4^+/CH_4 reaction.[7,8] We have recently studied the ArN_2^+/CH_4 reaction at thermal energy by using an ion-beam apparatus in order to examine the reactivity of the heteromolecular ArN_2^+ cluster ion.[9] Since only CH_4^+ due to CT was detected in the ArN_2^+/CH_4 reaction, the reactivity of ArN_2^+ was found to be similar to that of Ar_2^+ for CH_4. The reaction rate constant of ArN_2^+/CH_4 (0.90×10^{-9} $cm^3\,s^{-1}$) was similar to those of Ar_2^+/CH_4 (0.93×10^{-9} $cm^3\,s^{-1}$)[6] and N_4^+/CH_4 (0.90-1.0×10^{-9} $cm^3\,s^{-1}$).[7,8]

In the present study, a comparative mass spectroscopic study was conducted on the ion-molecule reactions between the ArN_2^+/n-C_4H_{10} and ArN_2^+/i-C_4H_{10} reactions at thermal energy. The product ion distributions and reaction rate constants are determined. The CT process of ArN_2^+/n-C_4H_{10} is discussed by reference to reported breakdown curves of the parent cation. The results obtained are compared with those for the CO_2^+/C_4H_{10} and Ar^+/C_4H_{10} reactions[10,11] to obtain information on the reactivity of the simple cluster ion. The RE's of CO_2^+ (13.78 eV) and Ar^+ (15.76 eV) are lower and higher than that of ArN_2^+ (14.51 eV), respectively.

Experimental

The thermal ion-beam apparatus used in the present study was essentially the same as that reported previously.[9—12] The apparatus consists of a flowing-afterglow ion source, a low-pressure reaction chamber, and a quadrupole mass spectrometer. The ground $Ar^+(^2P_{3/2})$ and metastable $(Ar^+)^*$ ions were generated by a microwave discharge of high purity Ar gas in a quartz flow tube, and N_2 was added about 10 cm downstream from the center of the discharge. The product ions were then expanded into an interaction chamber through an orifice centered on the flow tube axis. At low Ar buffer gas pressures, Ar^+ and N_2^+ were found as reactant ions, whereas besides these ions, Ar_2^+, ArN_2^+, N_3^+, and N_4^+ cluster ions were observed at high Ar buffer gas pressures. Among these ions, only the ArN_2^+ ion was strongly enhanced with increasing in the N_2 flow rate, because the equilibrium of the following reactions lies to the right:[5,13—15]

$$N_4^+ + Ar \leftrightarrow ArN_2^+ + N_2, \quad (1)$$

$$Ar_2^+ + N_2 \leftrightarrow ArN_2^+ + Ar. \quad (2)$$

The metastable $Ar(^3P_{0,2})$ atoms generated in the discharge were completely quenched by the $Ar(^3P_{0,2}) + N_2 \rightarrow N_2(C^3\Pi_u) + Ar$ excitation-transfer reaction[16,17] in the ion source before they entered the reaction chamber. The absence of the contribution of $Ar(^3P_{0,2})/C_4H_{10}$ Penning ionization was confirmed by the disappearance of product ion signals, when reactant ions in the source were trapped using an ion-collector grid placed between the microwave discharge and the orifice.

The sample gas was kept at a constant mass flow and injected from a stainless steel orifice placed 5 cm downstream from the nozzle. The reactant and product ions were sampled through a molybdenum orifice placed 3 cm further downstream and analyzed using a quadrupole mass spectrometer. The mass spectra were averaged using a digital storage oscilloscope and stored in a microcomputer. Typical operating pressures were 1.8 Torr (1 Torr=133.3 Pa) in the flowing-afterglow ion-source chamber, 3×10^{-3} Torr in the reaction chamber, and 2×10^{-5} Torr in the mass analyzing chamber.

Results and Discussion

Product Ion Distributions. Typical mass spectra obtained for the $ArN_2^+/n\text{-}C_4H_{10}$ and $ArN_2^+/i\text{-}C_4H_{10}$ reactions are shown in Fig. 1(a) and (b), respectively. In both spectra, $C_3H_n^+$ (n=5—7) and $C_4H_9^+$ are found. In addition, $C_2H_n^+$ (n=4,5) and $C_4H_{10}^+$ are detected in the $ArN_2^+/n\text{-}C_4H_{10}$ spectrum. Although $N_2CH_4^+$ resulting from displacement reaction has been obtained in the N_4^+/CH_4 reaction as a major product,[7,8] such a cluster ion cannot be detected in the reactions of ArN_2^+ with $n\text{-}C_4H_{10}$ and $i\text{-}C_4H_{10}$. In general, displacement reaction becomes significant when the ionization potential of a target molecule is either comparable with the RE of a reactant ion or higher than that.[18,19] On the other hand, only CT occurs when the ionization potential of a target molecule is lower than the RE of the reactant ion. Therefore, the lack of the displacement channels in the ArN_2^+/C_4H_{10} reactions is explained by the facts that the RE of ArN_2^+ (14.51 eV) is higher than the ionization potentials of $n\text{-}C_4H_{10}$ (10.55 eV) and $i\text{-}C_4H_{10}$ (10.57 eV).[20] As described later, the effective RE of ArN_2^+ is estimated to be ca. 13.5 eV, which is still much higher than the ionization potentials of $n\text{-}C_4H_{10}$ and $i\text{-}C_4H_{10}$.

In order to determine whether product ions are produced from the primary reaction or some secondary reactions, the dependence of branching ratios of each product ion on $n\text{-}C_4H_{10}$ flow rate is measured, as shown in Fig. 2. With increasing $n\text{-}C_4H_{10}$ flow rate,

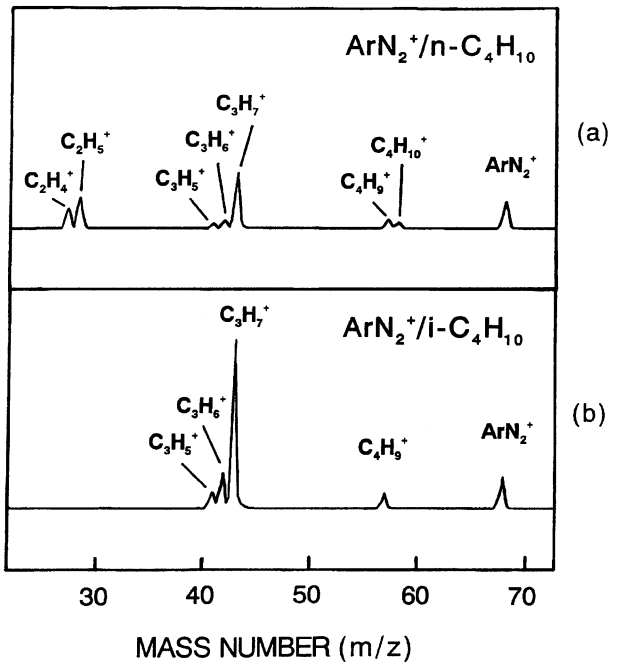

Fig. 1. Typical mass spectra resulting from the (a) $ArN_2^+/n\text{-}C_4H_{10}$ and (b) $ArN_2^+/i\text{-}C_4H_{10}$ reactions at thermal energy. The spectra are uncorrected for the relative sensitivity.

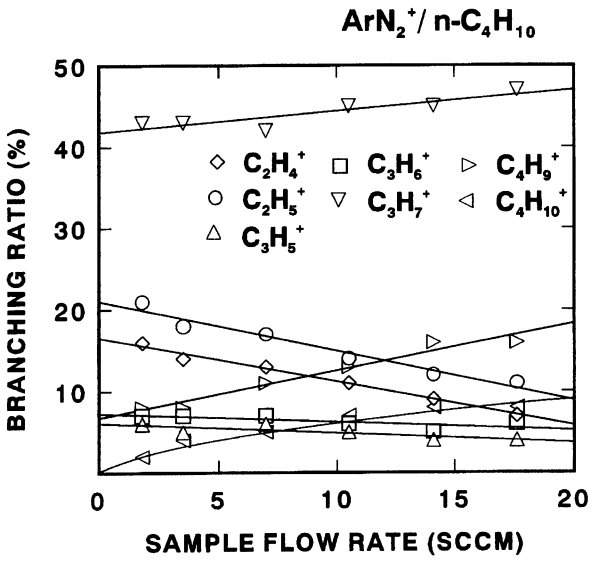

Fig. 2. The variation of the branching ratios of the ionic products with $n\text{-}C_4H_{10}$ flow for the $ArN_2^+/n\text{-}C_4H_{10}$ reaction.

the branching ratios of $C_3H_7^+$, $C_4H_9^+$, and $C_4H_{10}^+$ increase, while those of $C_2H_4^+$ and $C_2H_5^+$ rapidly decrease. Although the branching ratios of $C_3H_5^+$ and $C_3H_6^+$ decrease with increasing $n\text{-}C_4H_{10}$ flow rate, their reductions are small. By extrapolating the percentages of each product ion to zero $n\text{-}C_4H_{10}$ flow, the initial branching ratios of primary reactions (3a)—(3f) are determined:

$$ArN_2^+ + n\text{-}C_4H_{10} \rightarrow C_4H_9^+ + H + Ar + N_2, \quad (3a)$$

$$\rightarrow C_3H_7^+ + CH_3 + Ar + N_2, \quad (3b)$$

$$\rightarrow C_3H_6^+ + CH_4 + Ar + N_2, \quad (3c)$$

$$\rightarrow C_3H_5^+ + (CH_4 + H,\ CH_3 + H_2) + Ar + N_2, \quad (3d)$$

$$\rightarrow C_2H_5^+ + (C_2H_5,\ C_2H_4 + H) + Ar + N_2, \quad (3e)$$

$$\rightarrow C_2H_4^+ + C_2H_6 + Ar + N_2. \quad (3f)$$

The results obtained are given in Table 1 along with our previous data for the $CO_2^+/n\text{-}C_4H_{10}$ and $Ar^+/n\text{-}C_4H_{10}$ reactions.[10,11] The $C_4H_9^+$, $C_3H_n^+$ (n=5—7), and $C_2H_n^+$ (n=4,5) fragments occupy 6, 57, and 37% of the total product ions, respectively. These values are in good agreement with the corresponding values in the $CO_2^+/n\text{-}C_4H_{10}$ reaction, which gives 6, 56, and 38%, for $C_4H_9^+$, $C_3H_n^+$ (n=5—7), $C_2H_n^+$ (n=3—5), respectively. However, they are different from the data for the $Ar^+/n\text{-}C_4H_{10}$ reaction, in which higher branching fractions of smaller fragment ions such as $C_2H_5^+$ and $C_2H_3^+$ are found due to the higher RE of Ar^+.

Combining the data shown in Fig. 2 with the known reactions of the hydrocarbon system,[21] possible secondary reactions leading to $C_4H_{10}^+$, $C_4H_9^+$, and $C_3H_7^+$ are as follows:

Table 1. Product Ion Distributions in the ArN_2^+/C_4H_{10}, CO_2^+/C_4H_{10}, and Ar^+/C_4H_{10} Reactions and Photoionization of C_4H_{10}

Reactant molecule	Product ion	Appearance potential[a]	Branching ratio/%				
			ArN_2^+	CO_2^+	Ar^+	$h\nu$	
		eV	14.51 eV This work	13.78 eV Ref. 10	15.76 eV Ref. 11	13.0 eV Ref. 27	13.5 eV Ref. 27
n-C_4H_{10}	$C_4H_{10}^+$	10.55	0	0	0	13.83	12.31
	$C_4H_9^+$	11.65	6±1	6	0	1.89	1.80
	$C_4H_7^+$	12.51	0	0	0	0	0
	$C_3H_7^+$	11.19	44±4	25	0	61.92	58.34
	$C_3H_6^+$	11.16	7±1	5	0	6.36	6.30
	$C_3H_5^+$	13.40	6±1	26	22	0.82	2.84
	$C_2H_5^+$	12.55	21±2	22	36	5.20	7.58
	$C_2H_4^+$	11.65	16±2	13	10	9.57	10.07
	$C_2H_3^+$	13.66	0	3	32	0	0.21
i-C_4H_{10}	$C_4H_{10}^+$	10.57	0	0	0		
	$C_4H_9^+$	11.60	13±2	7	0		
	$C_3H_7^+$	11.23	68±4	53	1		
	$C_3H_6^+$	10.93	13±2	9	2		
	$C_3H_5^+$	<13.78[b]	6±1	31	42		
	$C_2H_5^+$	13.80	0	0	7		
	$C_2H_4^+$	11.65	0	0	2		
	$C_2H_3^+$	13.75	0	0	46		

a) Ref. 20. b) Ref. 10.

$$C_2H_4^+ + n\text{-}C_4H_{10} \rightarrow n\text{-}C_4H_{10}^+ + C_2H_4 + 0.10\ \text{eV}, \quad (4a)$$
$$\rightarrow n\text{-}C_4H_9^+ + C_2H_5 + 0.02\ \text{eV}, \quad (4b)$$
$$\rightarrow s\text{-}C_4H_9^+ + C_2H_5 + 0.76\ \text{eV}, \quad (4c)$$
$$\rightarrow n\text{-}C_3H_7^+ + i\text{-}C_3H_7 + 0.08\ \text{eV}, \quad (4d)$$
$$\rightarrow i\text{-}C_3H_7^+ + n\text{-}C_3H_7 + 0.64\ \text{eV}, \quad (4e)$$
$$\rightarrow i\text{-}C_3H_7^+ + i\text{-}C_3H_7 + 0.78\ \text{eV}, \quad (4f)$$

$$C_2H_5^+ + n\text{-}C_4H_{10} \rightarrow n\text{-}C_4H_9^+ + C_2H_6 + 0.38\ \text{eV}, \quad (5a)$$
$$\rightarrow s\text{-}C_4H_9^+ + C_2H_6 + 1.11\ \text{eV}, \quad (5b)$$

$$C_3H_5^+ + n\text{-}C_4H_{10} \rightarrow s\text{-}C_4H_9^+ + C_3H_6 + 0.33\ \text{eV}, \quad (6a)$$
$$\rightarrow i\text{-}C_3H_7^+ + C_4H_8 + 0.32\ \text{eV}. \quad (6b)$$

Here, the ΔH° values are calculated from reported thermochemical data.[20] The rate constants of processes (4), (5), and (6) have been estimated to be $(1.14\pm0.13)\times10^{-9}$, $(8.4\pm0.2)\times10^{-10}$, and $(5.0\pm0.6)\times10^{-10}$ $cm^3\,s^{-1}$, respectively, though the product ions have not been identified except for process (5).[21]

The branching ratios of the product ions in the ArN_2^+/i-C_4H_{10} reaction are independent of i-C_4H_{10} flow rate, as shown in Fig. 3. It is therefore concluded that all product ions are formed by the primary reactions under the operating conditions:

$$ArN_2^+ + i\text{-}C_4H_{10} \rightarrow C_4H_9^+ + H + Ar + N_2, \quad (7a)$$
$$\rightarrow C_3H_7^+ + CH_3 + Ar + N_2, \quad (7b)$$
$$\rightarrow C_3H_6^+ + CH_4 + Ar + N_2, \quad (7c)$$

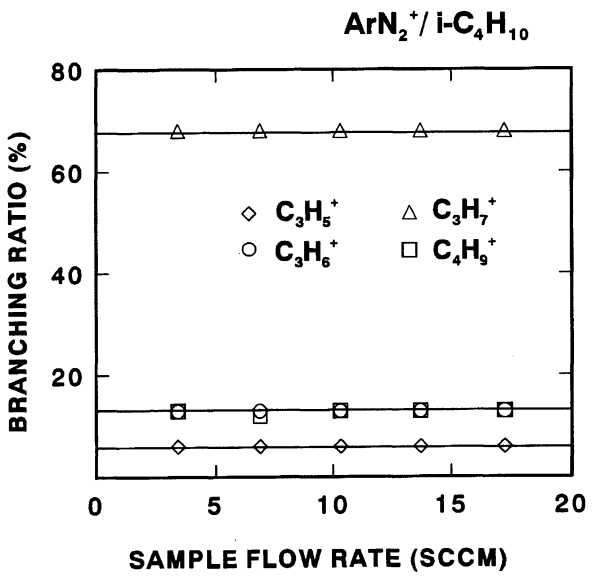

Fig. 3. The variation of the branching ratios of the ionic products with i-C_4H_{10} flow for the ArN_2^+/i-C_4H_{10} reaction.

$$\rightarrow C_3H_5^+ + (CH_4 + H,\ CH_3 + H_2) + Ar + N_2. \quad (7d)$$

The branching ratios of each product ion are given in Table 1 together with our previous data for the CO_2^+/i-C_4H_{10} and Ar^+/i-C_4H_{10} reactions.[10,11] The $C_4H_9^+$ and $C_3H_n^+$ (n=5—7) fragments occupy 13 and 87% of the total product ions, respectively. The branching ratio of $C_4H_9^+$ is about twice larger than that in the $CO_2^+/$

i-C_4H_{10} reaction, while the branching ratio of $C_3H_5^+$ reduces to one-fifth in comparison with that in the CO_2^+/i-C_4H_{10} reaction. The major product ions in the Ar^+/i-C_4H_{10} reaction are $C_3H_5^+$ and $C_2H_3^+$, which occupy 88% of the total product ions. The branching ratios of these smaller fragment ions are either small or zero in the ArN_2^+/i-C_4H_{10} reaction because of the lower RE of ArN_2^+. The most obvious feature in the ArN_2^+/i-C_4H_{10} reaction is the lack of $C_2H_n^+$ fragments. The $C_2H_n^+$ fragments can be easily formed from n-$C_4H_{10}^+$ by cleavage of C–C and C–H bonds without significant rearrangement of chemical bonds. Meanwhile, cleavage of two skeletal C–C bonds followed by creation of a new C–C bond is required for the formation of the $C_2H_n^+$ fragments from i-C_4H_{10}. Thus, the lack of $C_2H_n^+$ fragments from i-C_4H_{10} can be attributed to a low probability of significant rearrangement of chemical bonds through the CT reaction of ArN_2^+/i-C_4H_{10}.

Charge-Transfer Mechanism. The appearance potentials of each product ion are shown in Table 1. The appearance potential of $C_3H_5^+$ from i-C_4H_{10} had been measured as 14.55 eV under electron-impact ionization.[22] However, we have estimated it to be less than 13.78 eV because of the detection of $C_3H_5^+$ from the CO_2^+/n-C_4H_{10} reaction.[9] In the CT reactions of ArN_2^+ with n-C_4H_{10} and i-C_4H_{10}, fragment ions with appearance potentials of 10.93—13.78 eV are observed. All of these energies are lower than the RE of ArN_2^+ (14.51 eV).

Figure 4 shows breakdown curves of n-$C_4H_{10}^+$ obtained by Chupka and Lindholm using various reactant atomic and molecular ion beams with collisional energies of 5 and 900 eV.[23] The product ion distribution obtained in the thermal ArN_2^+/n-C_4H_{10} reaction does not agree with that predicted from breakdown curves at 14.51 eV. However, a good agreement is found between the observed distribution and the breakdown curves at ca. 13.2 eV, as shown in Fig. 4. It was therefore concluded that the product ions are formed through (pre)-dissociation of n-$C_4H_{10}^+$ states at ca. 13.2 eV.

Recent ab initio calculations of Hiraoka et al.[13] have demonstrated that the ArN_2^+ cluster ion has a linear structure in the stable geometry with centers of mass Ar–N_2 distance of ca. 2.8 Å, and 84% of the positive charge is located in Ar atom. The RE at an infinite Ar–N_2 distance is 14.51 eV. When ArN_2^+ accepts an electron, the resulting Ar–N_2 potential is repulsive at a short Ar–N_2 distance of 2.8 Å, so that the effective RE of ArN_2^+ becomes lower than 14.51 eV. Although the Ar–N_2 potential with a triangular configuration is more stable than that with a linear configuration,[25,26] the linear configuration is expected to be maintained at the instance of electron jump. In our preliminary experiments on the ion-molecule reactions of ArN_2^+ with such saturated hydrocarbons as C_2H_6 and C_3H_8,[24] it was found that most of all product ions are formed through (pre)dissociation of parent cations in the same energy

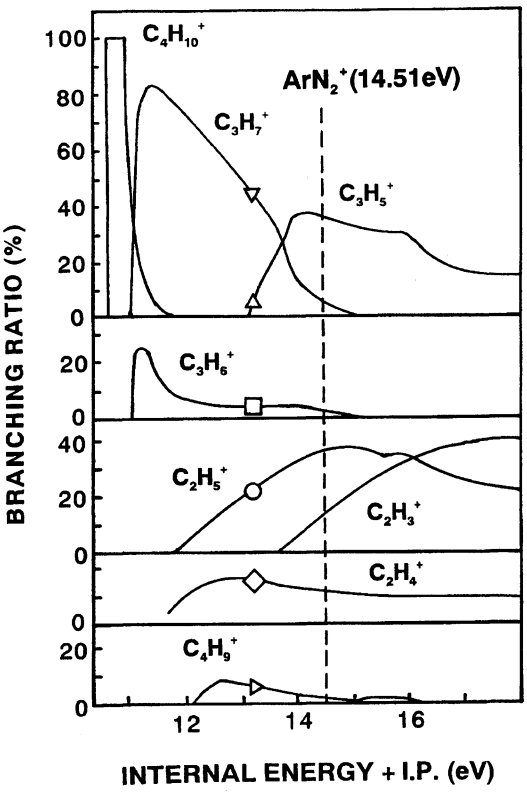

Fig. 4. Breakdown diagram of n-$C_4H_{10}^+$. Adopted from Ref. 23. Branching ratios of the ionic products in the ArN_2^+/n-C_4H_{10} reaction is shown at 13.2 eV.

range. On the basis of these findings, it is reasonable to assume that the CT reactions of ArN_2^+ with simple saturated hydrocarbons populate precursor ionic states at ca. 13.2 eV.

According to the theoretical and experimental studies of the ground-state Ar–N_2 potential by Bowers et al.[25] and Beneventi et al.,[26] the potential has a small well at an Ar–N_2 distance of 4.28 Å for a parallel configuration, and a strongly repulsive wall at shorter distances. By using parameters of Lennald–Jones (12, 6) potential measured by Beneventi et al.[26] the repulsive energy of Ar–N_2 at an Ar–N_2 distance of 2.8 Å is estimated to be 1.0 eV. Then, the effective RE of ArN_2^+ at an equilibrium Ar–N_2^+ distance of 2.8 Å is estimated to be ca. 13.5 eV. Since this energy is close to the observed energy of the precursor n-$C_4H_{10}^+$ states, the ArN_2^+/n-C_4H_{10} reaction must proceed through a near-resonant electron jump and the perturbation of the potential function of ArN_2^+ by approaching n-C_4H_{10} molecule is insignificant before an electron jump from n-C_4H_{10} to ArN_2^+.

The most obvious difference in the CT reactions of molecular ions in comparison with those of atomic ions is that the internal (vibrational and rotational) degrees of freedom in the reactant ions are acceptable modes of an excess energy, besides the internal degrees of freedom in product ion and translational degrees of freedom in products. If the excess energy is released statistically among all degrees of freedom in products, the possibility

of nonresonant CT would be large for molecular ions. However, we have recently found that the $Ar^+/n\text{-}C_4H_{10}$ and $CO_2^+/n\text{-}C_4H_{10}$ reactions proceed through similar near-resonant processes in which the breakdown of precursor $n\text{-}C_4H_{10}^+$ ion occurs near the RE's of Ar^+ (15.76 eV) and CO_2^+ (13.78 eV).[10,11] This implies that the internal degrees of freedom in CO_2^+ do not play a significant role in the CT mechanism of the $CO_2^+/n\text{-}C_4H_{10}$ reaction. Here, we found that the $ArN_2^+/n\text{-}C_4H_{10}$ CT reaction proceeds through a similar mechanism, where the effective RE of ArN_2^+ is efficiently converted into the ionization energy of $n\text{-}C_4H_{10}$ and internal energies of the $n\text{-}C_4H_{10}^+$ ion. Thus, the internal degrees of freedoms would be also insignificant in CT reactions of the ArN_2^+ cluster ion.

In order to compare the reactivity between the thermal CT and photoionization at comparable energies, the product ion distributions in photoionization at 13.0 and 13.5 eV[27] are shown in Table 1. Prominent features in the photoionization of $n\text{-}C_4H_{10}$ are high branching ratios of $n\text{-}C_4H_{10}^+$ and $C_3H_7^+$ in comparison with those of $C_2H_5^+$ and $C_2H_4^+$. Figure 5 shows photoelectron spectra (PES) of $n\text{-}C_4H_{10}$ and $i\text{-}C_4H_{10}$ reported by Kimura et al.[28] Since the photoionization initially populate ionic states with favorable Franck–Condon (FC) factors, the $n\text{-}C_4H_{10}^+$ states in the 11—13 eV region will be formed preferentially. According to the breakdown curves of $n\text{-}C_4H_{10}^+$, the parent $C_4H_{10}^+$ ion and the daughter $C_3H_7^+$ ion are major products in this energy region, which is in agreement with the photoionization data. The contribution of low energy ionic states below ca. 13 eV is insignificant in the $ArN_2^+/n\text{-}C_4H_{10}$ reaction, even though FC factors are large. Thus, the branching ratios of $C_4H_{10}^+$ and $C_3H_7^+$ with low appearance potentials become either small or zero in the $ArN_2^+/n\text{-}C_4H_{10}$ reaction.

There are nine ionic states of $n\text{-}C_4H_{10}^+$ in the 11—17 eV region based on PES shown in Fig. 5(a). In the caption of Fig. 5 are given vertical ionization potentials (IP_v) of each state, molecular orbitals of removal electrons, and their bonding characters reported by Kimura et al.[28] The $ArN_2^+/n\text{-}C_4H_{10}$ reaction initially populates ionic states near ca. 13.2 eV. Therefore, important precursor states of $n\text{-}C_4H_{10}^+$ are expected to be near-resonant states 4 and 5, arising from loss of a 2a″ electron with π_{CH_3} character and a 12a′ electron with σ_{CC} character, respectively. The nature of molecular orbitals of the removal electrons suggests that the major $C_2H_n^+$ fragments dominantly arise from cleavage of a C–C bond in state 5($12a'^{-1}$), while the minor $C_4H_9^+$ fragment arises from fission of a C–H bond in state 4-($2a''^{-1}$):

$$ArN_2^+ + n\text{-}C_4H_{10} \rightarrow n\text{-}C_4H_{10}^+(\text{state 5}) + Ar + N_2, \quad (8a)$$
$$\downarrow$$
$$C_2H_n^+(n = 3\text{–}5),$$

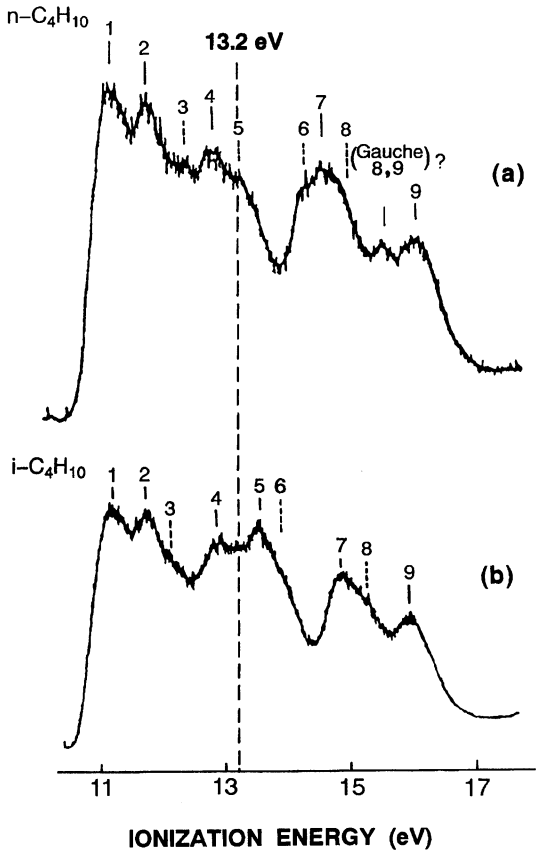

Fig. 5. Photoelectron spectra of $n\text{-}C_4H_{10}$ and $i\text{-}C_4H_{10}$. Adopted from Ref. 28. $n\text{-}C_4H_{10}$: Peak 1 (I_V=11.09 eV, 14a′, σ_{CC}), 2 (11.66 eV, 3a″, π_{CH_2}), 3 (12.3 eV, 13a′, σ_{CC}), 4 (12.74 eV, 2a″, π_{CH_3}), 5 (13.2 eV, 12a′, σ_{CC}), 6 (14.2 eV, 1a″, π_{CH_3}), 7 (14.59 eV, 11a′, π_{CH_3}), 8 (15.0 eV, 10a′, σ_{CC}), and 9 (15.99 eV, 9a′, π_{CH_2}), and $i\text{-}C_4H_{10}$: Peak 1 (I_V=11.13 eV, $6a_1$, σ_{CH}, σ_{CC}), 2 (11.70 eV, 5e, σ_{CC}), 3 (12.1 eV, 5e, σ_{CC}), 4 (12.85 eV, $1a_2$, π_{CH_3}), 5 (13.52 eV, 4e, π_{CH_3}), 6 (13.9 eV, 4e, π_{CH_3}), 7 (14.86 eV, 3e, π_{CH_3}), 8 (15.3 eV, 3e, π_{CH_3}), and 9 (15.95 eV, $5a_1$, π_{CH_3}).

$$\rightarrow n\text{-}C_4H_{10}^+(\text{state 4}) + Ar + N_2,$$
$$\downarrow$$
$$C_4H_9^+. \quad (8b)$$

Similar ionic states are present for $i\text{-}C_4H_{10}$, as shown in Fig. 5(b). Ionization mechanism is uncertain for the $ArN_2^+/i\text{-}C_4H_{10}$ reaction because the breakdown curve of $i\text{-}C_4H_{10}^+$ is unknown. However, it is highly likely that the reaction also proceeds through near-resonant CT. The most probable near-resonant precursor states of $i\text{-}C_4H_{10}^+$ are states 4 and 5, arising from loss of a $1a_2$ or 4e electron with the same π_{CH_3} character. Therefore, the major $C_3H_n^+$ ions are probably formed through cleavage of a C–H bond followed by C–C bond dissociation.

Rate Constants. Figure 6 shows semilogarithmic plots of ArN_2^+ ion current vs. reagent flow rate. Total rate constants $k_{C_4H_{10}}$ are determined from the decay of

Table 2. Observed and Calculated Reaction Rate Constants of the ArN_2^+/C_4H_{10}, CO_2^+/C_4H_{10}, and Ar^+/C_4H_{10} Reactions at Thermal Energy

Reactions		k_{obsd}	$k_{calcd}^{a)}$	k_{obsd}/k_{calcd}
		10^{-9} cm^3 s^{-1}		
$ArN_2^+ + n$-C_4H_{10}	This work	0.69±0.23	1.2	0.58±0.19
$ArN_2^+ + i$-C_4H_{10}	This work	0.90±0.26	1.2	0.75±0.22
$CO_2^+ + n$-C_4H_{10}	Ref. 10	0.98±0.20	1.3	0.75±0.15
$CO_2^+ + i$-C_4H_{10}	Ref. 10	1.0±0.2	1.3	0.77±0.15
$Ar^+ + n$-C_4H_{10}	Ref. 11	0.79±0.28	1.4	0.57±0.20
$Ar^+ + i$-C_4H_{10}	Ref. 11	0.86±0.31	1.4	0.62±0.22

a) Calculated from Langevin theory.

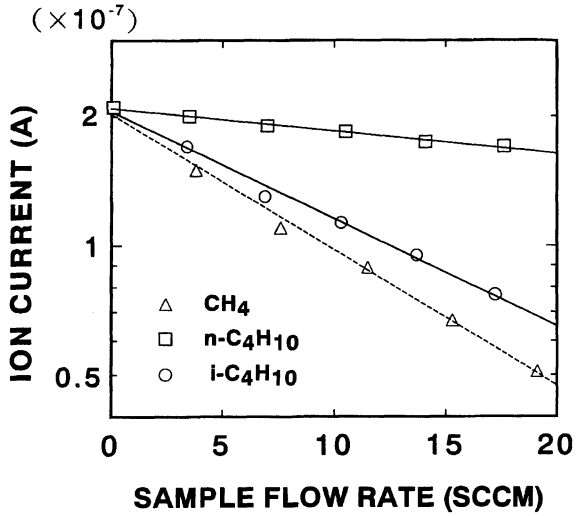

Fig. 6. The variation of the reactant ion current with the sample gas flow for the ArN_2^+/n-C_4H_{10} and ArN_2^+/i-C_4H_{10} reactions. As a reference the decay of ArN_2^+ upon addition of CH_4 under the same experimental conditions is shown.

ArN_2^+, which is governed by the pseudo-first-order rate law,

$$I(ArN_2^+) = I_0(ArN_2^+) \exp(-k_{C_4H_{10}}[C_4H_{10}]t). \quad (9)$$

Here, $I_0(ArN_2^+)$ represents the initial ArN_2^+ ion current and t is the reaction time. Because of the difficulty in evaluating the accurate t value, the $k_{C_4H_{10}}$ value is evaluated by reference to the rate constant of the ArN_2^+/CH_4 reaction (k_{CH_4}), which has recently been determined to be $(9.0\pm1.9)\times10^{-10}$ cm^3 s^{-1},[9]

$$k_{C_4H_{10}} = k_{CH_4} \frac{\ln\{I(ArN_2^+)/I_0(ArN_2^+)\}_{C_4H_{10}}}{\ln\{I(ArN_2^+)/I_0(ArN_2^+)\}_{CH_4}} \frac{[CH]_4}{[C_4H_{10}]}. \quad (10)$$

The decay of ArN_2^+ upon addition of CH_4 under the same experimental conditions is also shown in Fig. 6. The faster decay of ArN_2^+ for i-C_4H_{10} than that for n-C_4H_{10} implies that the rate constant of the ArN_2^+/i-C_4H_{10} reaction is larger than that of the ArN_2^+/n-C_4H_{10} one. The rate constants obtained from slopes in Fig. 6 are summarized in Table 2. Total rate contants of thermal-energy ion-molecule reactions have been evaluated by using the Langevin theory for non-polar molecules with small dipole moments[29] and the average dipole orientation (ADO) theory for polar molecules with large dipole moments.[30,31]

$$k_L = 2\pi e(\alpha/\mu)^{1/2} \quad (11)$$

$$k_{ADO} = (2\pi e/\mu^{1/2})[\alpha^{1/2} + C\mu_D(2/\pi kT)^{1/2}], \quad (12)$$

where α and μ_D are polarizability and dipole moment of C_4H_{10},[32] μ is a reduced mass of the reactant system, and C is a parameter given by Su and Bowers.[31] Since the μ_D values of n-C_4H_{10} (<0.05 D) and i-C_4H_{10} (0.132 D) are small, the k_{ADO} values are nearly the same as the k_L ones. Therefore, theoretical collision rate constants given in Table 2 were calculated by using Langevin theory. To the best of our knowledge, the α value of i-C_4H_{10} has not been reported. Thus, the k_L value for i-C_4H_{10} was calculated assuming that the α value of i-C_4H_{10} is identical with that of n-C_4H_{10}. The ratio of the observed and calculated rate constants serves as a measure for the efficiency of a reaction. Relatively high efficiencies of 58 and 75% are found for n-C_4H_{10} and i-C_4H_{10}, respectively. For comparison, the k_{obsd} values for the CO_2^+/C_4H_{10} and Ar^+/C_4H_{10} reactions are given in Table 2. The rate constant of the ArN_2^+/n-C_4H_{10} reaction is 23% smaller than that of the ArN_2^+/i-C_4H_{10} reaction. However, no significant differences are found in the k_{obsd} values among the ArN_2^+, CO_2^+, and Ar^+ reactions, indicating that electron jump occurs at similar interparticle distances.

Summary

Thermal energy reactions of ArN_2^+ with n-C_4H_{10} and i-C_4H_{10} have been investigated by using an ion-beam apparatus. The product distributions and rate constants were determined and summarized in Tables 1 and 2, respectively. For all reactions, only CT product channels were observed and no evidence of displacement

reaction was found. $C_4H_9^+$, $C_3H_n^+$ (n=5—7), and $C_2H_n^+$ (n=4,5) are produced from n-C_4H_{10} with branching ratios of 6, 57, and 37%, while $C_4H_9^+$ and $C_3H_n^+$ (n=5—7) are formed from i-C_4H_{10} with branching ratios of 13 and 87%, respectively. The lack of $C_2H_n^+$ fragments from i-C_4H_{10} is attributed to a low probability of significant rearrangement of chemical bonds for the formation of the $C_2H_n^+$ fragments. The product ion distributions led us to conclude that the ArN_2^+/n-C_4H_{10} reaction populates near-resonant n-$C_4H_{10}^+$ states at ca. 13.2 eV. The total rate constants correspond to 58 and 75% of the collision rate constants estimated from Langevin theory.

The authors are grateful to Professor Kenzo Hiraoka at Yamanashi University for his helpful discussion and providing his results before publication. This work was partly supported by the Iwatani Naoji Memorial Foundation and a Grant-in-Aid for Scientific Research No. 06453026 from the Ministry of Education, Science and Culture.

References

1) E. E. Ferguson, "Kinetics of Ion-Molecule Reactions," ed by P. Ausloos, Plenum, New York (1979).
2) "Vacuum Ultraviolet Photoionization and Photodissociation of Molecules and Clusters," ed by C. Y. Ng, World Scientific, Singapole (1991).
3) K. Norwood, J. H. Guo, and C. Y. Ng, *J. Chem. Phys.*, **90**, 2995 (1989).
4) M. F. Jarrold, A. J. Illies, and M. T. Bowers, *J. Chem. Phys.*, **81**, 214 (1984).
5) H. S. Kim and M. T. Bowers, *J. Chem. Phys.*, **93**, 1158 (1990).
6) R. J. Shul, B. L. Upschulte, R. Passarella, R. G. Keesee, and A. W. Castleman, Jr., *J. Phys. Chem.*, **91**, 2556 (1987).
7) D. Smith, N. G. Adams, and T. M. Miller, *J. Chem. Phys.*, **69**, 308 (1978).
8) J. L. McCrumb, A. B. Rakshit, and P. Warneck, *Ber. Bunsenges. Phys. Chem.*, **84**, 677 (1980).
9) M. Tsuji, K. Matsumura, H. Kouno, T. Funatsu, and Y. Nishimura, *J. Chem. Phys.*, **99**, 6215 (1993)
10) M. Tsuji, K. Matsumura, T. Funatsu, Y. Nishimura, H. Obase, S. Kagawa, and Y. Kanetaka, *Bull. Chem. Soc. Jpn.*, **66**, 2864 (1993).
11) M. Tsuji, K. Matsumura, T. Funatsu, H. Kouno, Y. Nishimura, H. Obase, S. Kagawa, Y. Kanetaka, H. Kugishima, and K. Yoshida, *J. Mass Spectrom. Soc. Jpn.*, **41**, 63 (1993).
12) M. Tsuji, H. Kouno, K. Matsumura, T. Funatsu, Y. Nishimura, H. Obase, H. Kugishima, and K. Yoshida, *J. Chem. Phys.*, **98**, 2011 (1993).
13) K. Hiraoka, T. Mori, and S. Yamabe, *Chem. Phys. Lett.*, **189**, 7 (1992).
14) H. H. Teng and D. C. Conway, *J. Chem. Phys.*, **59**, 2316 (1973).
15) K. Hiraoka, private communication.
16) T. D. Nguyen and N. Sadeghi, *Chem. Phys.*, **79**, 41 (1983).
17) N. Sadeghi, M. E. Cheaib, and D. W. Setser, *J. Chem. Phys.*, **90**, 219 (1989).
18) D. Smith and N. G. Adams, *Chem. Phys. Lett.*, **161**, 30 (1989).
19) K. Giles, N. G. Adams, and D. Smith, *J. Phys. B*, **22**, 873 (1989).
20) H. M. Rosenstock, K. Draxl, B. W. Steiner, and J. T. Herron, *J. Phys. Chem. Ref. Data*, **6**, Suppl. 1 (1977).
21) Y. Ikezoe, S. Matsuoka, M. Takebe, and A. Viggiano, "Gas-Phase Ion-Molecule Reaction Rate Constants through 1986," Maruzen, Tokyo (1987), and references therein.
22) I. Omura, *Bull. Chem. Soc. Jpn.*, **34**, 1227 (1961).
23) W. A. Chupka and E. Lindholm, *Ark. Fys.*, **25**, 349 (1963).
24) M. Tsuji, K. Matsumura, H. Kouno, T. Funatsu, and Y. Nishimura, to be published.
25) M. S. Bowers, K. T. Tang, and J. P. Toennies, *J. Chem. Phys.*, **88**, 5465 (1988).
26) L. Beneventi, P. Casavecchia, G. G. Volpi, C. C. K. Wong, and F. R. W. McCourt, *J. Chem. Phys.*, **98**, 7926 (1993).
27) J. W. Au, G. Cooper, and C. E. Brion, *Chem. Phys.*, **173**, 241 (1993).
28) K. Kimura, S. Katsumata, Y. Achiba, T. Yamazaki, and S. Iwata, "Handbook of HeI Photoelectron Spectra of Fundamental Organic Molecules," Japan Sci. Soc. Press, Tokyo (1981).
29) G. Gioumousis and D. P. Stevenson, *J. Chem. Phys.*, **29**, 294 (1958).
30) T. Su and M. T. Bowers, *Int. J. Mass Spectrom. Ion Phys.*, **12**, 347 (1973).
31) T. Su and M. T. Bowers, *Int. J. Mass Spectrom. Ion Phys.*, **17**, 211 (1975).
32) "CRC Handbook of Chemistry and Physics," 68th ed, ed by R. C. Weast, M. J. Astle, and W. H. Beyer, CRC Press, Florida (1987—1988).